Baas Andreas CW (Orcid ID: 0000-0001-9305-5868)

Jackson Derek DW (Orcid ID: 0000-0003-1778-2187)

Using wind run to predict sand drift

Andreas CW Baas[1*], Derek DW Jackson[2], Irene Delgado-Fernandez[3], Kevin Lynch[4], J Andrew G Cooper[2]

[1] Department of Geography, King's College London, London, UK
[2] Centre for Coastal and Marine research, School of Environmental Sciences, University of Ulster, Coleraine, UK
[3] Department of Geography, Edge Hill University, Ormskirk, UK
[4] School of Geography and Archaeology, National University of Ireland, Galway, Ireland

* Correspondence to: Andreas CW Baas, Department of Geography, King's College London, Bush House, 30 Aldwych, London WC2B 4BG, United Kingdom, +44 (0)20 7848 2421, andreas.baas@kcl.ac.uk

Abstract

Conventional aeolian sand transport models relate mass transport rate to wind speed or shear velocity, usually expressed and empirically tested on a 1-second time-scale. Projections of total sand delivery over long time-scales based on these models are highly sensitive to any small bias arising from statistical fitting on empirical data. We analysed time-series of wind speed and sand transport rate collected at 14 independent measurement stations on a beach during a prior field experiment. The results show that relating total sand drift to cumulative above-threshold wind run yields models which are more statistically robust when fitted on empirical data, generating smaller prediction errors when projected to longer time-scales. Testing of different power exponents indicates that a linear relationship between sand drift and above-threshold wind run yields the best results. These findings inspire a speculative novel phenomenological model relating the mass flow of air in the boundary layer to the mass transport of sand over the surface.

Keywords

aeolian sand transport, regression, prediction, statistical analysis, phenomenological model

Running head: USING WIND RUN TO PREDICT SAND DRIFT

This article has been accepted for publication and undergone full peer review but has not been through the copyediting, typesetting, pagination and proofreading process which may lead to differences between this version and the Version of Record. Please cite this article as doi: 10.1002/esp.4848

Introduction

Accurate prediction of the amount of sand moved by wind is a key ambition in our pursuit toward a better understanding of the physical mechanisms and processes involved, and it is vital for practical applications relating to sediment budgets on coasts and arid lands, dust emissions, and dune dynamics. Over the years several dozen equations and models have been developed to express sand transport rate as a function of wind forcing (speed or shear velocity). Dong *et al.* (2003), for example, compared and categorized 19 predictive equations. The majority of these relate bulk sand transport rate Q, in terms of mass shifted across a lateral span per unit time, e.g. kg m^{-1} s^{-1}, to the cube of shear velocity of the boundary layer airflow, U_*^3. Most equations also explicitly include a shear velocity threshold of motion for sand grains, U_{*t}, below which no sand is moved. The models underlying the equations consider sand transported in saltation mode only and the cubic relationship to U_* partly rests on an assumption that the speed of saltating grains is proportional to U_*. This is now thought to be a weak dependency so some recent models relate sand transport rate to U_*^2 instead (Martin & Kok 2017; Duran *et al.* 2011).

Direct comparison of common transport equations, using the best estimates of empirical coefficients and threshold values, shows a great divergence between predictions, ranging over nearly an order of magnitude for any given shear velocity (Sherman and Li 2012). More disconcerting, however, is that the majority of field studies testing predictive equations against direct measurements indicate a poor performance of these equations altogether (e.g. Arens 1996, Wiggs 2011, Bauer *et al.* 1990), with measured transport rates ranging anywhere from 65% to 300% of predicted rates (Ellis & Sherman 2013). The comparisons are confounded by the fact that accurate and synchronous empirical measurement of sand transport as well as wind forcing in field experiments is challenging (Baas 2008); i.e. both sides of the comparison suffer from significant error bars.

While most equations are derived from theoretical models and calibrated in wind tunnels, empirical studies try to statistically fit their functional mathematical forms to measurements of sand transport rate and wind forcing. Analysis by Davidson-Arnott *et al.* (2009), for example, shows a large variation in fitted exponents for empirical power-law relationships between wind speed and sand transport intensity measured with electronic probes at 1 Hz. More generic polynomials can also be applied, as shown in the work by Jackson and McCloskey (1997) fitting a parabolic equation through 1 Hz field data, with good results. The fitting and testing of sand transport equations is usually conducted at this short time-scale of 1 second but this is also the time-scale that exhibits great spatio-temporal variability in sand transport in response to wind turbulence and surface conditions, yielding inescapable mismatches between models and measurements (Barchyn *et al.* 2014). Temporal scale impacts on the resultant wind forcing variable, particularly determination of shear velocity, and on the assessment of thresholds, while it has also been shown that the correlation between wind forcing and sand transport response generally improves at longer time-scales (Martin *et al.* 2013).

This study attempts to address one of the fundamental challenges of contemporary aeolian sand transport models: the problem of projecting predictions based on transport equations that are designed and tested on a temporal scale of seconds to the much longer time-scales needed to assess sand delivery to foredunes or infrastructure over the course of months and years.

Wind speed or Wind run

With traditional sand transport equations that are empirically fitted or calibrated on a time-scale of seconds, any minor error or bias, i.e. over-estimation or under-estimation, is severely amplified when projecting to time-scales of weeks, months, or years, as it spans over many orders of magnitude.

The analysis presented here explores an alternative approach for relating sand transport to wind forcing, by considering these variables in cumulative form: relating wind run to sand drift. Wind run is defined as the total length of airflow (in metres) that has passed through, i.e. wind speed integrated over time. Sand drift is defined here as the total amount of sand that has been moved across a unit width (in mass m^{-1}), i.e. sand transport rate integrated over time. The cumulative approach should be equivalent to the normal, "differential," approach, since wind run and sand drift need to be, in practice, assessed over some specific duration. For example, wind run after a month is equivalent to the average wind speed for that month multiplied by the number of seconds in a month, and the total sand drift can similarly be converted from the average sand transport rate. While theoretically equivalent, the question is, however, whether the statistical fitting through empirical data may be different and possibly more robust in the cumulative form rather than the differential form, so that the cumulative form may be used for more accurate prediction of sand delivery over long periods of time.

As an initial exploration of this alternative on relatively short time-scales, we compare the statistical performance of the cumulative wind run model and the differential wind speed model fitted through empirical data collected in a field experiment at 25 Hz at fourteen independent measurement locations. The two models are fitted for integer power exponents and include a fitted transport threshold, such that:

for wind run: $$Q = m\,(WR_{>Ut})^n \quad [1]$$

where: Q is sand drift (g m^{-1}), m is the slope coefficient, $WR_{>Ut}$ is wind run (m) exceeding a wind speed threshold, U_t , and n is an integer exponent; and

for wind speed: $$q = m\,U^n + b \quad [2]$$

where: q is sand transport rate (g m^{-1} s^{-1}), m is the slope coefficient, U is wind speed (m s^{-1}), b is the offset, and n is an integer exponent. The wind speed threshold can be derived from the fitted parameters via:

$$U_t = \left(\frac{-b}{m}\right)^{1/n} \quad [3]$$

The two models are fitted on three different time scales spanning two orders of magnitude: 1 s, 10 s, and 100 s.

Study site and methods

Instrumentation

The data analysed here was collected during field experiments on the beach of Magilligan Strand, Northern Ireland (Figure 1), as part of a larger research project on airflow reversal by foredunes under offshore winds (Jackson *et al.* 2011, 2013). The data were collected during a measurement run on the 3rd of May 2010 under oblique *onshore* wind, with a similar set-up as that described in Lynch *et al.* (2013). The beach is oriented along a north-west – south-east axis, facing the sea toward the north-east, and is backed by foredunes of up to 12 m in height. The beach is flat and up to 100 m wide during spring low tides. The sediment consists of mono-disperse, very well sorted, fine-grained quartz sand, with a median grain size, D_{50}, of 0.17 mm, a sorting value of 0.3 ϕ (very well sorted) and a skewness of 0.15 (fine skewed) (Folk & Ward 1957). The beach was relatively free of debris and vegetation at the time of the experiments.

[Figure 1 roughly here]

Wind and sand transport were synchronously measured at twenty stations distributed in a grid over the dry beach surface (Figure 2). At each station wind was measured with a Gill HS-50 sonic anemometer, mounted at 0.5 m above the surface, recording 3D wind vectors at 25 Hz, and sand transport was measured with a collocated continuously weighing horizontal sediment trap (Figure 3). This trap is a modified form of the Jackson trap (1996) with a 3.5 kg capacity load-cell, outputting the increasing weight of accumulating sand inside the trap over time. The saltating sand falls into the trap over a 0.25 m diameter funnel opening that is flush with the surface, with the load-cell bucket and electronics buried underneath. All instruments were connected to a custom-made data acquisition system recording all data at 25 Hz with synchronous time stamps.

[Figure 2 roughly here]

The grid of stations was organised over four cross-shore transects spaced at 30 m alongshore intervals. Within transects A, C, and D four stations were spaced at 10 m intervals from the back beach towards the shore. Transect B had an increased spatial resolution with eight stations spaced at 5 m intervals. Station B2 included a mast with four sonic anemometers, but the analysis presented here uses only the instrument mounted at 0.5 m. This grid was overseen by a reference sonic anemometer, unaffected by topography, mounted at 6 m above the foredune crest (18 m above the beach surface).

[Figure 3 roughly here]

Data-processing

Data were subjected to strict quality control standards and this yielded a period of 4000 seconds (67 minutes) of reliable continuous time-series at 25 Hz of both 3D wind vectors and cumulative sand capture, recorded synchronously. Quality control criteria included the integrity and continuity of the wind data (no gaps), and monotonically increasing trap data (no negative changes and no reverberations). The wind conditions measured above the foredune crest show a mean oblique onshore wind flow direction of 44 degrees away from shore-normal, i.e. nearly exactly diagonal onto the shoreline, as a northerly wind in Figure 1. Five-second averaged wind direction data indicate a normal distribution around this mean with a standard deviation of 7 degrees, which suggests that 95% of the wind was contained within a window ±14 degrees on either side of the diagonal mean wind direction. Trap data posed the main limitation to quality control, including some traps

approaching the load-cell capacity after 4000 seconds and others experiencing communication problems, leading to some stations being excluded from analysis. Fourteen stations passed quality control and are used in this study: A1-3, B1-6, C1-3, D1 and D3.

A minimal trapping efficiency correction was applied to the trap data to take into account saltating grains that have long-enough horizontal trajectory lengths to jump over the 0.25 m diameter round funnel opening. We used COMSALT (Kok & Renno 2009) to simulate a population of more than 27,000 instances of saltating and reptating grains with a diameter of 0.17 mm (the D_{50} at the site), driven by a shear velocity of 0.4 m s^{-1} (roughly twice the transport threshold, see below) and including the effects of turbulence. This generated a statistical distribution of horizontal trajectory lengths. Applying this distribution to the trapping distance across the circular opening, varying from 0.25 m at the centre-line to zero at the edges, and integrating over the lateral width of the trap, shows that overall 25% of the saltating sand is able to jump over the hole. Trapping efficiency thus amounts to 75% and sand capture data were adjusted by a factor of 4/3 accordingly. The sand trap data were then multiplied by four to convert from the 0.25 m width of the trap to a standard unit metre width.

The 3D sonic anemometry data were adjusted to a true horizontal plane based on the angle from vertical reported by each on-board inclinometer sensor. Because the analysis considers only horizontal wind speed (and not Reynolds shear stress, for example) no streamline correction was applied. Data of windspeed and cumulative sand capture at each station were resampled to 10 Hz, as the temporal response of the trap load-cell is limited to this time scale. We then determined the optimum lag between wind speed fluctuations and transport rate response at each station and applied this to allign the time-series with maximum correlation (lags ranged from 0.6 to 1.1 seconds). This provided the baseline dataset from which we produced paired time-series with periods of 1 s, 10 s, and 100 s, by resampling from the 10 Hz time-series of wind speed and cumulative sand capture. For the wind run method the data need no further conversions as the trap data are already in cumulative form. For the wind speed method the cumulative sand capture time-series are converted to a differential time-series to yield transport rates in grams per second per metre width.

Statistical analysis: wind run method

For this method a threshold is deducted from the wind speeds, and all resulting negative values reduced to zero. The excess wind speeds are then converted to wind run by multiplying each excess speed value by the length of the relevant period. The power-law exponent is applied to the wind run values and the time-series is converted to cumulative form. This is the x-variable in a least-squares linear regression with the y-variable being the cumulative sand trapped, and with the linear model fit forced through the origin (no offset parameter). The empirical data points are thus defined as:

$$x(t) = \sum_0^t [T\ (U - U_t)_{>0}]^n \qquad [4]$$

where: t is in time-steps of the relevant period T (1, 10, or 100 seconds), and

$$y(t) = M_{trap}(t) - M_{trap}(0) \qquad [5]$$

where: $M_{trap}(t)$ is the mass of sand collected in the trap at time t.

The evaluation statistics returned by the linear regression include the goodness-of fit, R^2, and the root mean square error, RMSE (reported here in g m^{-1}). In order to find the best-fit wind speed threshold the preceding calculations are repeated for a range of threshold values (from 2 to 6 m s^{-1} with a resolution of 0.01 m s^{-1}) and the eventual best-fit model is identified as the one with the lowest RMSE.

Statistical analysis: wind speed method

For this method transport rate measurements that are zero or very small need to be removed from the data set, as they are effectively 'noise' along the bottom of the scatter plot that adversely affect the regression models. Based on visual evaluation of scatter plots a filter threshold of 0.1 g s^{-1} m^{-1} was established to remove the low-level noise (later in the analysis we assess the impact of the filter threshold on the fitted model results). In general, the amount of transported sand that was removed as low-level noise amounts to roughly 0.1% of the total amount of sand trapped and can be considered negligible. The filtered transport rate measurements are the y-variable in a least-squares linear regression with the x-variable being the average windspeed raised to the power, *n*. The empirical data points are thus defined as:

$$x(t) = \left(\frac{1}{T}\sum_{t-T}^{t} U\,\Delta t\right)^{n} \quad [6]$$

where: *T* is the relevant period, and

$$y(t) = \frac{1}{T}\left[M_{trap}(t) - M_{trap}(t-T)\right] \quad [7]$$

The linear regression yields both a slope and an offset coefficient, and the offset can be converted to the equivalent threshold wind speed via equation [3]. The goodness-of-fit, R^2, returned by the linear regression can be compared with that of the wind run method. The RMSE, however, we calculate separately from the deviations between the modelled transport and observed transport data *in cumulative form* (i.e. RMSE in g m^{-1}), so that this measure is directly comparable to that obtained with the wind run method.

Transport threshold

Both methods yield an estimated sand transport threshold wind speed (at 0.5 m above the surface). In order to judge its sensibility in comparison with theoretical predictions and previous studies, the threshold wind speed is converted to a shear velocity, U_{*t}, by assuming a logarithmic law-of-the-wall velocity profile and a roughness length, z_0, estimated as Nikuradse's (1933): $k_s/30$, where k_s is taken to be $5 \times D_{50}$.

For reference: Bagnold's (1941) commonly applied threshold shear velocity formula:

$$U_{*t} = A\sqrt{g\,D\,\frac{\rho_s - \rho_a}{\rho_a}} \quad [8]$$

(where: *g* is gravitational acceleration (m s^{-2}), *D* is grain size (m), ρ_s and ρ_a are density of sand mineral – taken to be quartz – and air, respectively) predicts a threshold of 0.15 - 0.18 m s^{-1}, depending on whether the coefficient *A* is taken to be 0.8 for the continuation of transport (impact threshold), or 1.1 for initiation of saltation (fluid threshold).

Results

Figure 4 shows examples of the two model types fitted through data at an individual station for the three temporal scales, demonstrating the different nature of the two methods, where the traditional approach fits a cubic curve through a scatter plot of data, while the wind-run model fits a line through a cumulative trace. In graphical format, the traditional method is more intuitive because it relates transport rate (g/s) to a wind speed (m/s), whereas the independent axis on the wind-run graph here reflects cumulative above-threshold wind-run – a much harder variable to relate to. A more intuitive version is to graph cumulative transport versus plain wind-run, as in Figure 5, which reflects the time sequence of sand transport activity, showing periods of below-threshold winds (and no transport) as parts where the curve is horizontal. Such a graph is not useful for fitting or visualising a statistical model however.

[Figure 4 roughly here]

[Figure 5 roughly here]

For the practical application of predicting total amounts of sand delivered after certain events or periods of time (a storm, or a year), the cumulative total is the value of interest. The wind-run model yields this value directly, whereas for the scatter-plot method the fitted model must be integrated over time. Figure 6 demonstrates the key issue: inevitable minor bias in the fitted scatter-plot model is amplified and projected over a longer period, leading to a gradually increasing divergence between the predicted total sand delivery and the observed.

[Figure 6 roughly here]

The results of the statistical analysis are reported in Table 1, comparing the fitting of a cubic model on wind speed (n=3) via the traditional scatter plot regression and a linear model (n=1) on wind run via the cumulative trace. Models with other powers were also explored (see below), but the two reported in Table 1 were deemed the best performing ones. The results show that the cumulative wind run model provides a better statistical performance than the differential scatter model on all three time-scales and at all stations. The goodness-of-fit for the wind-run model is always greater than 0.99, while these values for the scatter plot method range from 0.82 to 0.97 even for the 100 s (the best performing) time-scale. The statistical performance of the wind speed model is poor at the 1 s time-scale, better at 10 s, and good at 100 s. Statistical performance of the wind-run model is consistently high at all three time-scales. These trends are evident in both the goodness-of-fit (R^2) and the RMSE. The RMSE measure is more informative, however, because it provides better discrimination among model fits with very high R^2 values. The U_{*t} values produced by the regression models all lie in the range of 0.16 to 0.20 m/s, across all time-scales and for both model types. This is in excellent agreement with the predicted range of thresholds from equation [8] and shows both that the model fittings are sensible and that a wind speed threshold predicted from that equation in conjunction with z_0 estimated as: $5\,D_{50}/30$ can be assumed from the outset for the wind run model. Difference in the methods is reflected in the sample size (N). In the wind-run model all data points are used in the statistical fit. The scatter-plot model, on the other hand, requires filtering of a

substantial number of measurements of very small or zero transport rates in order to produce acceptable statistical results.

[Table 1 roughly here]

Different powers

The statistical performance of model fits was assessed for different powers (*n* in equations 2 and 3) from 1 to 4, for each of the time-scales. Table 2 reports the averages across the 14 stations for the measures of goodness-of-fit (R^2) and the RMSE of the cumulative function. The results are somewhat ambiguous as they do not identify a straightforward optimal power for either of the model types, as trends vary depending on time-scale and depending on the performance measure. For wind-run models the RMSE is minimised at *n*=1 for the two shorter time-scales, but at *n*=2 for the 100 s period. Differences in R^2 values meanwhile are too small to allow differentiation. For scatter-plot models the highest R^2 values are achieved at *n*=4 for all three time-scales, but minimum RMSE at the 1 s period at *n*=1 and for 10 s and 100 s periods at *n*=3.

[Table 2 roughly here]

Model generality

Transferability of fitted models between stations was evaluated by taking the statistically fitted model derived from one station and applying it to the wind data at other stations to yield predicted cumulative sand displacement, compared against observed sand displacement. For the sake of brevity this analysis was only performed for the wind-run model with *n*=1 and for the wind speed model with *n*=3 (as these were deemed to be marginally the best overall performances in Table 2 in terms of RMSE). Table 3 reports the averages of the RMSE values resulting from all cross-applications (182 per time-scale) for the two model types, as well as the minimum and maximum within each set. The results show that RMSE values are similar for both types and that averages are an order of magnitude larger than the RMSE associated with the original model fitting themselves (Table 2). The range of error is quite large in both cases, with maximum RMSE exceeding 4.5 kg m^{-1} deviation between predicted and observed sand delivery (while sand displacement over the whole period amounted to about 7 kg m^{-1} on average across the stations). There are however also many cross-applications that produce very small RMSE. At the 100 s time-scale, for example, both model types see nearly 25% of cross-applications yielding an RMSE of less than 400 g m^{-1}. These results reflect the significant challenges of applying a statistically-fitted transport model derived at one location to another location, even within the same beach environment and wind conditions.

[Table 3 roughly here]

Predictive power

The predictive power of the two methods was explicitly tested by fitting cubic wind-speed and linear wind-run models to 1 s data from the first 400 seconds only (the first 10% of the time-series). The fitted model parameters were then applied to the full wind time-series to predict the total amount of sand drift after 4000 s, compared to the total amount observed. The results reported in Table 4 confirm the superior performance of the wind-run method to yield a predicted total sand drift after 4000 seconds that is closer to the observed amount, with errors (in absolute terms) of only 5-10% at

most stations (10 out of 14), whereas the wind-speed method results in prediction errors of 19% or more at most stations (10 out of 14). At all but one station the wind-run model yields a smaller error in sand drift prediction than the wind-speed model, and in most cases by many multiples at that. The thresholds that are determined from both types of fitted model, meanwhile, are similar to those from the previous full-data fitting (Table 1) at the 1 s time-scale. This suggests that the model fits are otherwise quite sensible and that the worse prediction error from the wind-speed method is a consequence of any minor bias of that model derived from the first 400 seconds being amplified when it is projected to 4000 seconds.

[Table 4 roughly here]

Discussion

It is not surprising that the wind run model shows better statistical fit in terms of R^2 than the scatter plot regressions: in the latter any outlier data points quickly degrade the goodness-of-fit, whereas in the wind run model these only lead to very small deviations in the cumulative trend. More fundamentally the key difference is that in the cumulative analysis the data points that are fitted through the regression are *not* mutually independent (as they are in the traditional scatter plot regression). The RMSE results, however, indicate a more robust fitting with smaller deviations in the cumulative form for the wind-run model, as compared with wind speed. At the coarsest time-scale the differences in statistical performance between the two methods narrow. It is to be expected that results converge: as the time-scale gets closer to the length of the dataset the wind run and the wind speed scatter become more identical, since average wind speed is equal to wind run divided by the sampling duration. Even then, while involving only ~30 data points, the wind run model shows better results at the 100 s time-scale.

It is particularly revealing how bias in the scatter plot regressions derived on small time-scales multiplies to significant estimation errors in the longer term: a cubic wind speed model fitted on 1 Hz data from 400 seconds of time-series leads to an estimation error of 23%, on average, of total sand drift when projected to 4000 seconds, whereas a linear wind run model fitted on 1 Hz data yields only a 11% difference, on average. The superiority of the wind-run model to predict total sand drift based on a short time-series is demonstrated at nearly all of the 14 stations in this field experiment. A strength of the analysis presented here is that findings can be tested and replicated over a large number of independent measurement stations rather than rely on just a single location or instance, as most other studies do.

In mathematical terms the two methods are analytically linked: wind run is an integration of wind speed over time, and so theoretically the exponent *n* for the wind run model ought to be one integer larger than the exponent on the wind speed model. The results in table 2 do not clearly support this expectation however. Differences in statistical performance at various *n* are relatively small, but for wind speed *n*=3 appears the best choice, also considering this conforms to the traditional model. This choice mathematically suggests *n*=4 for the wind run model, but on statistical measures that would be suboptimal. The linear model (*n*=1) appears a better solution, also because of its simplicity.

Advantages and disadvantages

The advantages of the wind run method include: *i)* more robust estimation of total sand drift over longer periods of time, and *ii)* simpler analysis, particularly for the linear model and when assuming the transport threshold predicted by equation [8] from the outset. Disadvantages include: *i)* graphical presentation less intuitive for visualising physical relationship, and *ii)* continuous time-series required.

In comparison, advantages of the traditional wind speed method include: *i)* intuitive graphical presentation, and *ii)* based on independent measurement points, while disadvantages include: *i)* bias extrapolates to significant error in predicting total sand drift over longer periods of time, *ii)* more complicated analysis and assumptions required for filtering of near-zero transport data and adjusting time-series for lags, particularly at short time-scales.

The main argument of the analysis exercise presented here is not to claim that the wind run model is altogether better, but to show that if we want to use empirical data on short time-scales as a basis for predicting sand delivery over longer periods, the cumulative analysis method is more statistically robust and reduces the potential for error due to bias magnification when upscaling.

Limitations and future work

The main limitation of the analysis exercise here is the relatively small range of time-scales considered, spanning only across three orders of magnitude, from seconds to thousands of seconds, with the upper limit imposed by the trap capacity being reached after ~1 hour of active sand transport. This study furthermore only concerns transport limited conditions, whereas surface conditions and supply limitations are crucial to upscaling and predicting sand drift over months or years. Nevertheless, in those applications the problems associated with calculating projections of total sand delivery based on predictive transport equations that have been empirically fitted on second-scale data remains, and our study shows that the wind run approach is more statistically robust. Future work should explore the application of the wind run method on longer time-scales, for example to estimate total sand drift over several weeks from hourly data, although it may prove harder to assure continuous transport limited conditions rather than supply controls.

Speculative phenomenological model

While presented here principally as an alternative data analysis method, the wind run model of equation [1] may also form the basis for hypothesising a physical sand drift model by considering dimensional analysis of the linear version of the equation (n=1) to attach meaning to the slope coefficient m. Equation 1 can be reflected in terms of the fundamental SI units of mass (M), length (L), and time (T) involved, adopting the method of directed dimensions (Huntley, 1967), where subscripts x, y, and z indicate length dimensions in streamwise, spanwise, and vertical directions:

$$\frac{M}{L_y} = [m]\, L_x \qquad [9]$$

with the dimensions of the coefficient m to be defined.

We may interpret the equation to represent a balance in mass transfer, per unit width, of sand (on the left-hand side) relative to air (on the right-hand side). The mass transfer of air is equivalent to the volumetric wind run multiplied by the density of air, ρ_a. This requires a vertical length scale to

define a 'depth' of flow, which we interpret as the height of the boundary layer, δ. The mass transfer of air per unit width is then equal to ρ_a *WR* δ, with dimensional analysis showing:

$$\left[\rho_a \, WR \, \delta\right] = \frac{M}{L_x \, L_y \, L_z} \, L_x \, L_z = \frac{M}{L_y} \qquad [10]$$

This suggests that the coefficient *m* can be treated as a non-dimensional coefficient, which the results in Table 1 indicate is of *O* (1). The model further requires a scaling of the height of measurement, *H*, as wind run is longer when measured higher above the ground. In the context of the volumetric transfer of air this may be considered as a fraction of the flow depth, i.e. the boundary layer height, yielding a dimensionless adjustment factor δ/H. The relationship between wind run and measurement height is technically of a logarithmic form (mirroring the velocity profile in the boundary layer flow), but if $H \gg z_0$ the linear simplification may be considered adequate.

A speculative phenomenological model for predicting total sand drift as a function of wind run may thus be formulated as:

$$Q \; = \; C \, \rho_a \frac{\delta^2}{H} \, WR_{>Ut} \qquad [11]$$

where: *C* is a calibration coefficient, and the positive dependency of sand drift on δ may be reflective of the fetch effect (Delgado-Fernandez 2010).

Conclusions

Traditional sand transport equations that are calibrated on statistical regression models of empirical data at short time-scales are less suitable for predicting total amounts of sand drift over longer periods of time, as any small bias is drastically magnified when upscaling, leading to significant estimation errors. An alternative analysis method using the cumulative approach of *wind run*, instead of wind speed, yields more robust statistical fitting of empirical data and smaller deviations in predicted total sand drift. Results presented here suggest that sand drift as a linear function of above-threshold wind run is the most effective, with the threshold derived from the customary Bagnold's (1941) equation in conjunction with a surface roughness length estimated as $5 \, D_{50}/30$.

The cumulative approach further inspires a speculative phenomenological model for predicting total sand drift as a function of above-threshold wind run (equation 11), including an explicit dependency on the height of the boundary layer.

References

Arens, S.M. (1996) Rates of aeolian transport on a beach in a temperate humid climate. Geomorphology 17, 3–18.

Baas, A.C.W. (2008) Challenges in aeolian geomorphology: Investigating aeolian streamers, Geomorphology 93, 3-16.

Bagnold, R. A. (1941) The Physics of Blown Sand and Desert Dunes, 265 pp., Chapman and Hall, London.

Barchyn, T.E., Martin, R.L., Kok, J.F. and Hugenholtz, C.H. (2014) Fundamental mismatches between measurements and models in aeolian sediment transport prediction: The role of small-scale variability. Aeolian Research, 15, pp.245-251.

Bauer, B.O., Sherman, D.J., Nordstrom, K.F., Gares, P.A. (1990) Aeolian transport measurement and prediction across a beach and dune at Castroville, California. In: Nordstrom, K.F., Psuty, N.P., Carter, R.W.G. (Eds.) Coastal Dunes: Form and Process. John Wiley, Chichester, pp.39–55.

Davidson-Arnott, R., Bauer, B.O., Walker, I.J., Hesp, P.A., Ollerhead, J. and Delgado-Fernandez, I. (2009) Instantaneous and mean aeolian sediment transport rate on beaches: an intercomparison of measurements from two sensor types. Journal of Coastal Research, pp.297-301.

Delgado-Fernandez, I. (2010) A review of the application of the fetch effect to modelling sand supply to coastal foredunes. Aeolian Research, 2(2-3), pp.61-70.

Dong, Z. B., X. P. Liu, H. T. Wang, and X. M. Wang (2003) Aeolian sand transport: a wind tunnel model, Sedimentary Geology, 161(1-2), 71-83.

Duran O, Claudin P and Andreotti B (2011) On aeolian transport: grain-scale interactions, dynamical mechanisms and scaling laws. Aeolian Res. 3 243–70

Ellis, J.T., Sherman, D.J. (2013) Fundamentals of Aeolian sediment transport: wind-blown sand. In: Shroder, J. (Editor in Chief), Lancaster, N., Sherman, D.J., Baas, A.C.W.(Eds.), Treatise on Geomorphology. Academic Press, San Diego, CA, vol.11, Aeolian Geomorphology, pp. 85-108

Folk, R.L. and Ward, W.C. (1957) Brazos River bar [Texas]; a study in the significance of grain size parameters. Journal of Sedimentary Research 27, 3-26.

Huntley, H. E. (1967), Dimensional Analysis, Dover Publications.

Jackson, D.W.T. (1996) A new, instantaneous aeolian sand trap design for field use. *Sedimentology*, *43*(5), pp.791-796.

Jackson, D.W. and McCloskey, J. (1997) Preliminary results from a field investigation of aeolian sand transport using high resolution wind and transport measurements. Geophysical Research Letters, 24(2), pp.163-166.

Jackson, D.W.T., Beyers, J.H.M., Lynch, K., Cooper, J.A.G., Baas, A.C.W. and Delgado-Fernandez, I. (2011) Investigation of three-dimensional wind flow behaviour over coastal dune morphology under offshore winds using computational fluid dynamics (CFD) and ultrasonic anemometry. *Earth Surface Processes and Landforms*, *36*(8), pp.1113-1124.

Jackson, D.W., Beyers, M., Delgado-Fernandez, I., Baas, A.C., Cooper, A.J. and Lynch, K. (2013) Airflow reversal and alternating corkscrew vortices in foredune wake zones during perpendicular and oblique offshore winds. Geomorphology, 187, pp.86-93.

Kok, J.F. and Renno, N.O. (2009) A comprehensive numerical model of steady state saltation (COMSALT). Journal of Geophysical Research: Atmospheres, 114(D17).

Lynch, K., Delgado-Fernandez, I., Jackson, D.W., Cooper, J.A.G., Baas, A.C. and Beyers, J.H.M. (2013) Alongshore variation of aeolian sediment transport on a beach, under offshore winds. Aeolian Research, 8, pp.11-18.

Martin, R.L., Barchyn, T.E., Hugenholtz, C.H. and Jerolmack, D.J. (2013) Timescale dependence of aeolian sand flux observations under atmospheric turbulence. *Journal of Geophysical Research: Atmospheres*, *118*(16), pp.9078-9092.

Martin, R.L. and Kok, J.F. (2017). Wind-invariant saltation heights imply linear scaling of aeolian saltation flux with shear stress. Science Advances, Vol. 3, no. 6, e1602569.

Nikuradse, J. (1933) Strömungsgesetze in rauhen Rohren, VDI-Forschungsheft, beilage zu Forschung auf dem Gebiete de Ingenieurswesens, heft 361, Ausgabe B(Band 4).

Sherman, D.J. and Li, B. (2012). Predicting aeolian sand transport rates: A reevaluation of models. Aeolian Research, 3(4), 371-378.

Wiggs, G.F.S. (2011) Sediment mobilisation by the wind. Chapter 18 in, Thomas, D.S.G. (ed.) (2011) Arid Zone Geomorphology: Process, Form and Change in Drylands, 3rd Edition. Wiley, 648 pp. ISBN: 9780470519080.

Acknowledgements

We thank Jasper Kok for providing guidance on using the COMSALT model. The field work was conducted as part of a research project funded by the UK Natural Environment Research Council (NE/F019483/1). The authors declare no conflicts of interest.

Data Availability Statement

The data that support the findings of this study are available from the corresponding author upon reasonable request.

Figure 1: Location of the field experiment in Northern Ireland, UK. Red box on map indicating location of Google Earth imagery shown in main panel. White box indicating location of field experiment measurement array. Scale bar equal to 1 km.

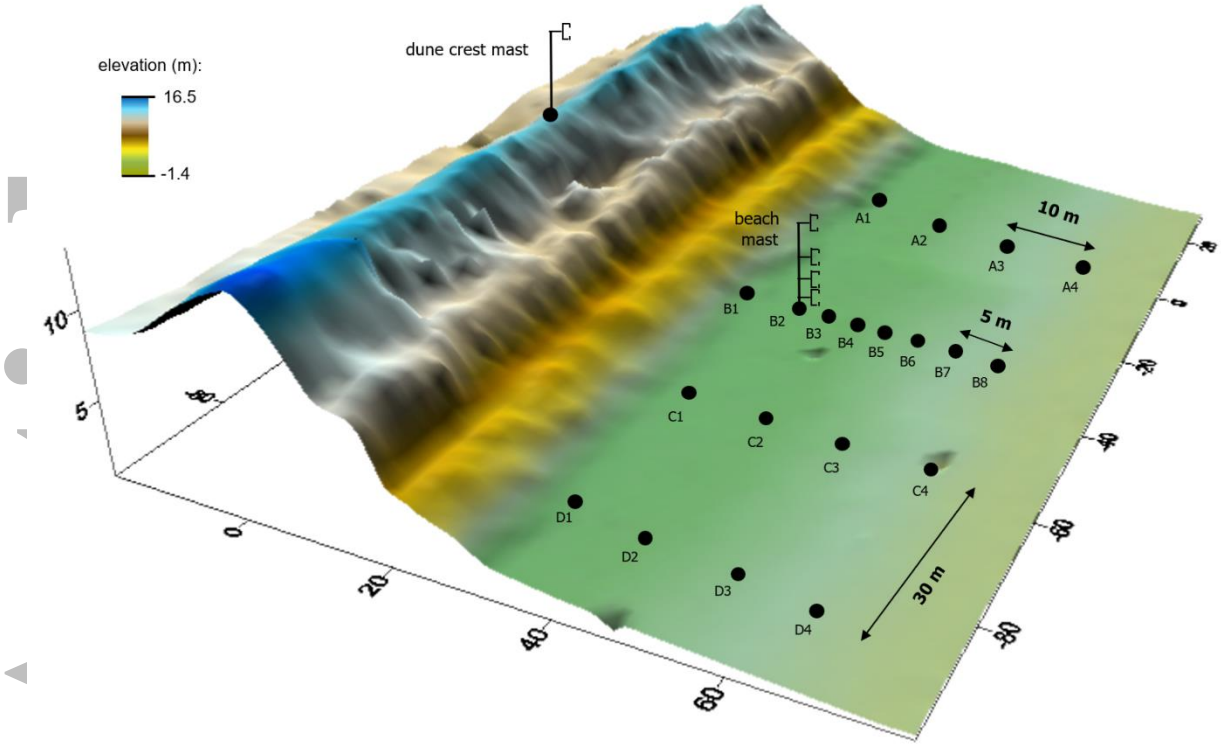

Figure 2: 3D map of the array of measurement stations, with rows A, B, C, and D running from dune foot seaward. Spacing between stations indicated.

Figure 3: view of measurement stations along row B, looking landward. Forefront shows sonic anemometer mounted at 0.5 m above the ground and buried sand trap indicated by inverted funnel (trap inactive at time of picture taken).

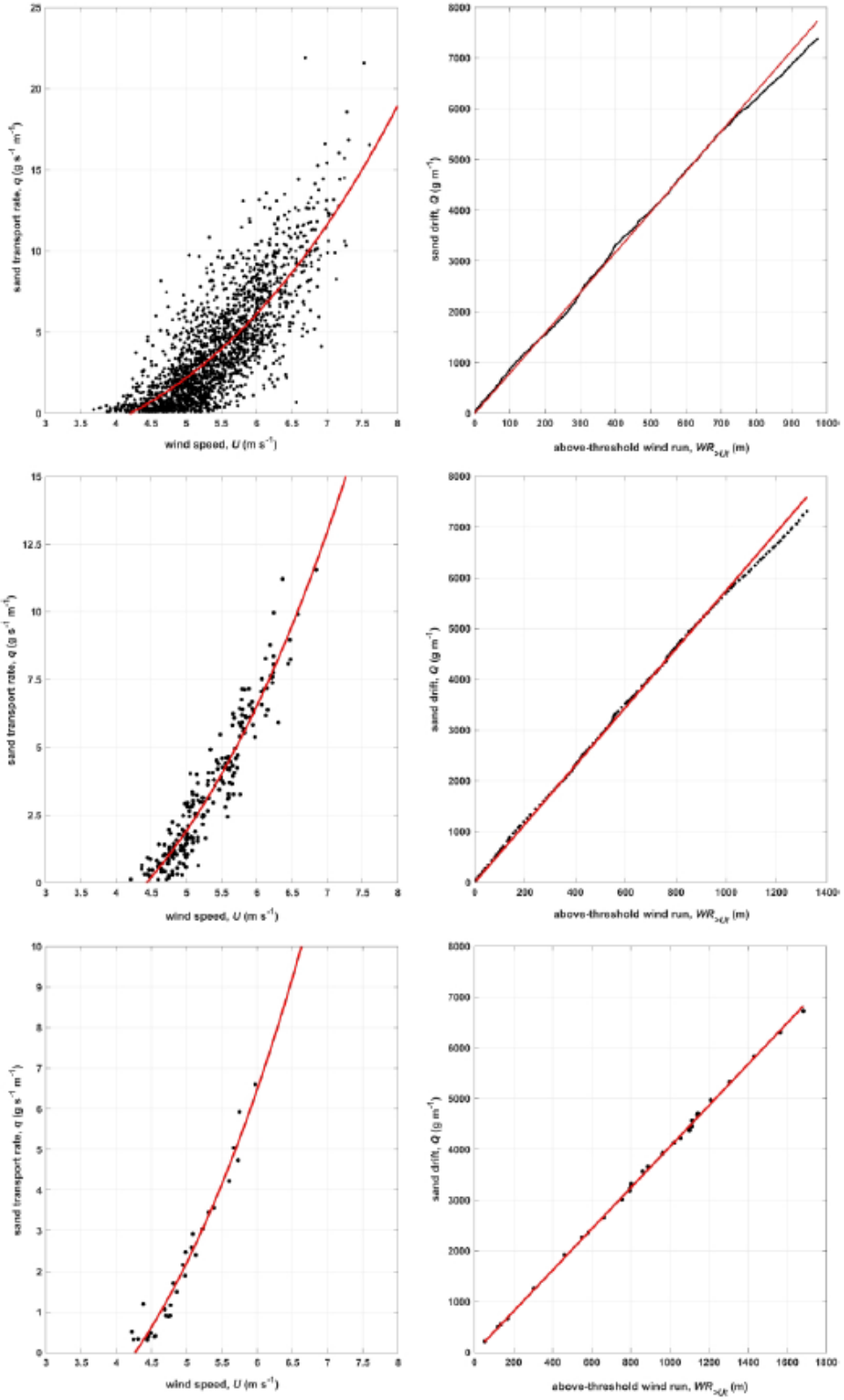

Figure 4: Examples of fitting a cubic wind speed model (left) and a linear above-threshold wind run model (right) to sand transport data, on time scales of 1 second (top), 10 seconds (middle), and 100 seconds (bottom). Black points are empirical data from station B6, red curves are model fitted via least-squares regression.

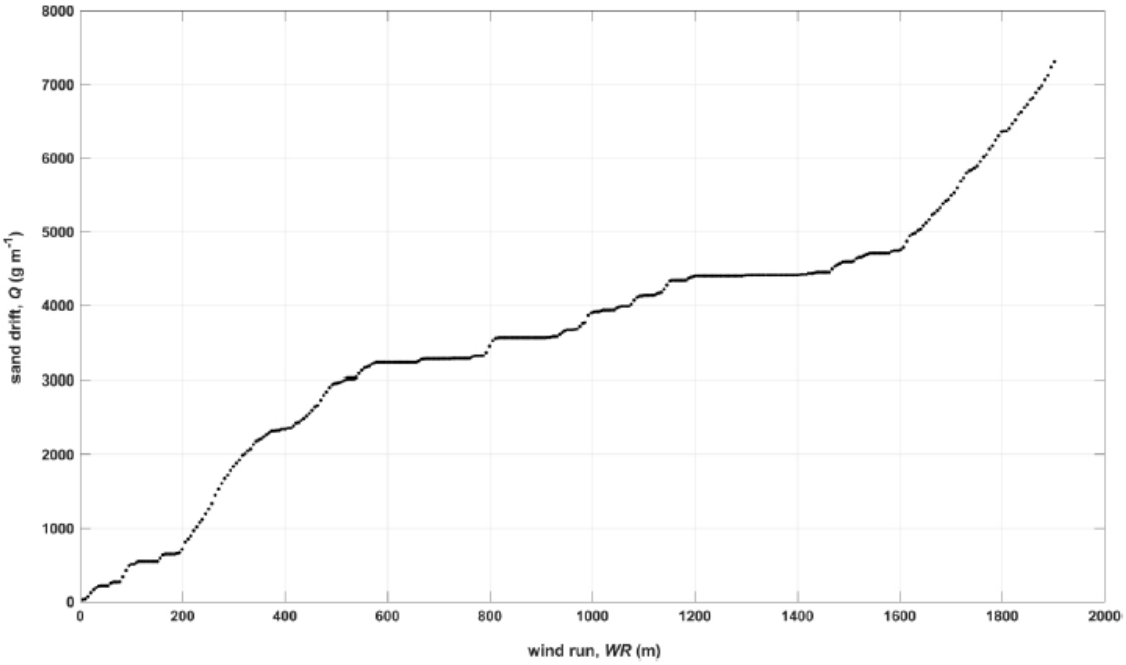

Figure 5: Trace of cumulative sand drift as a function of wind run (without threshold) for station B6 on a data time-scale of 10 seconds.

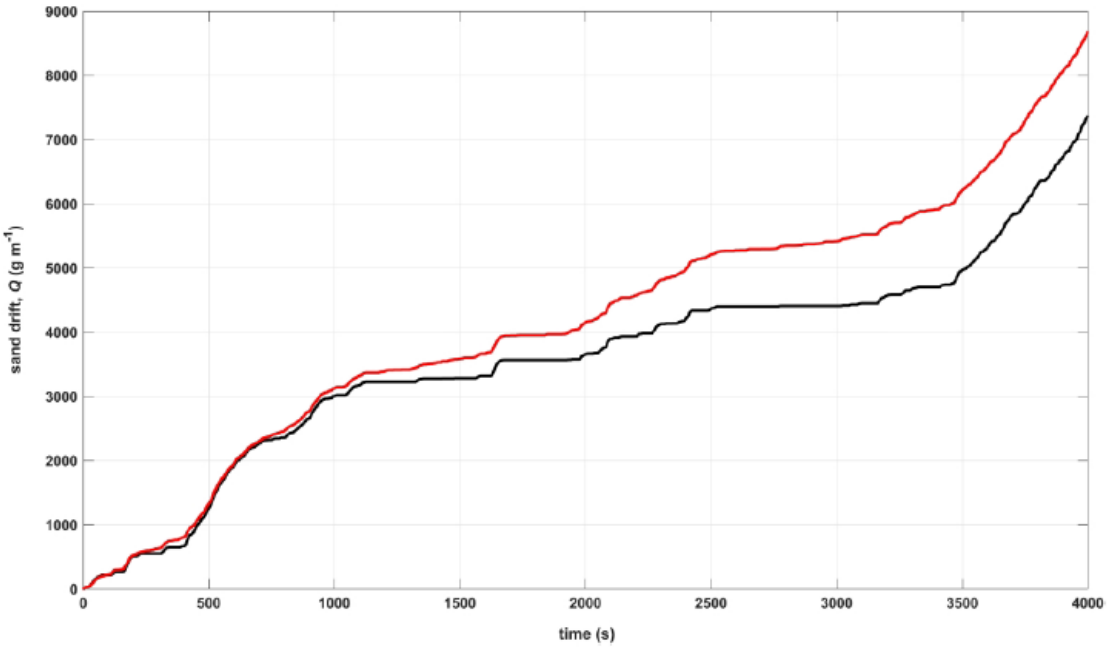

Figure 6: Cumulative sand drift as projected by integrating a cubic wind speed model (red) fitted on empirical data at 1 second time-scale, compared with the observed sand drift (black), for station B6.

Table 1: Results of fitting linear wind run and cubic wind speed models via regression on empirical data from 14 measurements stations on three different time scales. See text for explanation of variables.

	wind run - linear					wind speed - cubic				
station	**N**	**R^2**	**RMSE** ($g\ m^{-1}$)	**m**	**U*t** ($m\ s^{-1}$)	**N**	**R^2**	**RMSE** ($g\ m^{-1}$)	**m**	**U*t** ($m\ s^{-1}$)
A1	3999	0.999	25.3	6.62	0.20	1503	0.364	1542.9	0.032	0.15
A2	3999	0.995	108.4	6.59	0.20	1977	0.514	841.9	0.037	0.16
A3	3998	1.000	21.8	6.38	0.20	2170	0.564	1073.1	0.039	0.16
B1	3999	0.995	26.0	7.14	0.21	959	0.507	533.8	0.033	0.17
B2	3999	0.999	40.8	6.55	0.20	1528	0.315	1857.8	0.032	0.13
B3	3999	0.999	43.4	6.40	0.19	2072	0.471	1263.7	0.040	0.14
B4	3998	1.000	31.0	6.14	0.19	1919	0.566	889.8	0.041	0.16
B5	3998	0.997	90.1	6.34	0.20	2083	0.625	578.1	0.037	0.16
B6	3999	0.997	85.1	7.94	0.21	1873	0.642	744.6	0.043	0.17
C1	3999	1.000	27.9	7.33	0.18	2009	0.537	1079.7	0.047	0.14
C2	3999	0.998	89.3	8.46	0.20	2511	0.693	777.7	0.039	0.16
C3	3999	0.997	96.3	7.17	0.19	1870	0.686	952.3	0.050	0.16
D1	3998	0.999	26.4	4.29	0.20	2317	0.621	481.7	0.030	0.17
D3	3999	0.998	57.1	8.92	0.20	2114	0.625	588.7	0.039	0.17
mean:	**3999**	**0.998**	**54.9**	**6.88**	**0.20**	**1922**	**0.552**	**943.3**	**0.039**	**0.16**
A1	399	0.998	42.9	3.58	0.19	206	0.752	264.7	0.046	0.18
A2	399	0.998	73.4	5.32	0.19	239	0.852	121.0	0.048	0.18
A3	399	1.000	21.1	5.27	0.19	250	0.863	264.4	0.050	0.18
B1	399	0.992	34.0	2.58	0.18	154	0.774	119.1	0.038	0.18
B2	399	0.999	35.3	4.53	0.18	205	0.755	219.2	0.049	0.17
B3	399	1.000	29.6	5.18	0.18	256	0.808	230.9	0.052	0.17
B4	399	1.000	23.9	4.89	0.18	239	0.885	144.3	0.051	0.17
B5	399	0.997	80.6	4.92	0.19	244	0.885	112.3	0.043	0.17
B6	399	0.998	73.7	5.75	0.19	220	0.905	129.4	0.051	0.18
C1	399	1.000	24.7	5.50	0.17	235	0.851	171.4	0.065	0.16
C2	399	0.998	93.9	7.05	0.19	288	0.890	218.0	0.049	0.17
C3	399	0.998	78.1	5.47	0.18	228	0.920	128.4	0.060	0.17
D1	399	1.000	19.9	3.30	0.19	263	0.896	79.7	0.038	0.18
D3	399	0.998	58.8	7.39	0.19	250	0.888	134.8	0.048	0.18
mean:	**399**	**0.998**	**49.3**	**5.05**	**0.19**	**234**	**0.852**	**167.0**	**0.049**	**0.18**
A1	39	0.997	56.3	2.32	0.17	34	0.879	121.4	0.038	0.17
A2	39	0.997	80.7	3.83	0.18	34	0.957	125.2	0.044	0.17
A3	39	0.999	58.6	4.25	0.18	33	0.971	55.4	0.051	0.17

B1	39	0.984	46.2	1.61	0.17	22	0.821	74.3	0.029	0.16
B2	39	0.999	43.8	3.11	0.17	31	0.935	43.9	0.045	0.17
B3	39	0.998	66.7	3.90	0.17	34	0.967	59.8	0.054	0.16
B4	39	0.999	45.5	3.74	0.17	33	0.973	60.2	0.048	0.16
B5	39	0.998	71.5	3.47	0.17	33	0.957	143.8	0.040	0.17
B6	39	0.999	51.9	4.06	0.18	31	0.958	71.1	0.047	0.18
C1	39	0.999	58.2	4.15	0.16	34	0.955	64.1	0.062	0.16
C2	39	0.997	99.7	5.12	0.18	35	0.929	166.6	0.050	0.17
C3	39	0.999	45.9	3.98	0.17	35	0.951	60.2	0.056	0.17
D1	39	0.999	34.2	2.37	0.18	34	0.965	55.6	0.035	0.17
D3	39	0.993	113.0	3.86	0.18	34	0.930	173.9	0.048	0.17
mean:	**39**	**0.997**	**62.3**	**3.56**	**0.17**	**33**	**0.939**	**91.1**	**0.046**	**0.17**

Table 2: Averages across the 14 stations of the statistical performance of wind run and wind speed models with power exponent *n* ranging from 1 to 4, on each of the three time-scales.

		wind run		wind speed	
		R^2	RMSE	R^2	RMSE
n=1	**1 s**	0.998	54.9	0.524	856.8
	10 s	0.998	49.3	0.827	179.5
	100 s	0.997	62.3	0.909	102.4
n=2	**1 s**	0.998	64.2	0.542	865.3
	10 s	0.998	57.3	0.843	167.0
	100 s	0.997	56.9	0.927	93.1
n=3	**1 s**	0.997	72.1	0.552	943.3
	10 s	0.998	64.7	0.852	167.0
	100 s	0.997	60.5	0.939	91.1
n=4	**1 s**	0.997	78.2	0.554	1135.1
	10 s	0.997	70.2	0.853	187.0
	100 s	0.997	63.0	0.947	91.4

Table 3: Descriptive statistics of the RMSE (of the cumulative trace, in grams) for the cross-application of linear wind run and cubic wind speed models obtained from fitting on empirical data at one station and then applied to all other stations.

	wind run - linear			wind speed - cubic		
	mean	**min**	**max**	**mean**	**min**	**max**
1s	1090	26	4702	1384	115	5050
10s	1110	35	4561	1081	37	4691
100s	1154	54	4640	1106	56	4644

Table 4: Results of projecting models fitted on the first 10% of data (at 1 s time-scale) to predict total sand drift after the full 4000 seconds of measurements, comparing predicted to observed amounts, expressed as an absolute prediction error (where error = (predicted - observed)/observed).

			wind run - linear				wind speed - cubic		
station	**observed** (g)		**projected** (g)	**|error|**	**U_{*t}** (m s^{-1})		**projected** (g)	**|error|**	**U_{*t}** (m s^{-1})
A1	5165		5440	5 %	0.22		7578	47 %	0.14
A2	7471		7990	7 %	0.20		9003	21 %	0.17
A3	9294		9173	1 %	0.19		10370	12 %	0.15
B1	1801		1143	37 %	0.19		1971	9 %	0.14
B2	5596		7872	41 %	0.21		8854	58 %	0.12
B3	7691		7662	0 %	0.19		9224	20 %	0.14
B4	7156		7329	2 %	0.18		8514	19 %	0.15
B5	7156		7499	5 %	0.18		8123	14 %	0.16
B6	7374		8143	10 %	0.19		9444	28 %	0.17
C1	7564		9220	22 %	0.20		9279	23 %	0.14
C2	9205		10643	16 %	0.16		11628	26 %	0.15
C3	8393		8732	4 %	0.20		9974	19 %	0.17
D1	5471		5311	3 %	0.20		5642	3 %	0.17
D3	6377		6773	6 %	0.19		7576	19 %	0.17
mean:				**11 %**	**0.19**			**23 %**	**0.15**

Using wind run to predict sand drift

Andreas CW Baas[1*], Derek DW Jackson[2], Irene Delgado-Fernandez[3], Kevin Lynch[4], J Andrew G Cooper[2]

Conventional aeolian sand transport models based on wind speed or shear velocity are expressed and tested on a 1-second time-scale. These models can generate large errors when predicting total sand delivery over longer periods due to the amplification of any small bias. An alternative method relating total sand drift to cumulative above-threshold wind-run yields smaller prediction errors. These findings inspire a speculative phenomenological model relating the mass flow of air in the boundary layer to the mass transport of sand.